Influence of Laser Beam Power and Scanning Speed on the Macrostructural Characteristics of AISI 316L and AISI 431 Stainless Steel Depositions Produced by Laser Cladding Process

E.W.A. Figueredo, L.H.R. Apolinario, M.V. Santos, A.C.S. Silva, J.A. Avila, M.S.F. Lima, and T.F.A. Santos

In the laser cladding process, control of the process parameters and knowledge of the characteristics of the materials used are essential for obtaining depositions with excellent metallurgical union, satisfactory dilution values, absence of defects, and acceptable geometric characteristics. Without such precautions, depositions can exhibit low or excess dilution, low wettability, and the presence of pores, consequently reducing the performance of the materials. The aim of the present work was to evaluate the effects of the laser beam power, with maximum power of 4000 W and continuous wave mode, and scanning speed in laser cladding processes employing the AISI 316L austenitic stainless steel and the AISI 431 martensitic stainless steel, considering the geometric characteristics, dilution, and structural defects of the depositions. It was found that the laser power had a greater effect on the width and dilution of the depositions, while the scanning speed influenced the deposition height. The depositions of AISI 431 steel presented dilution values between 9 and 25%, using power settings between 1400 and 1600 W. The depositions of AISI 316L steel required higher power values between 1900 and 2600 W to achieve dilution values between 15 and 41%. The existence of pores and satisfactory hardness values were observed for both materials, with the average of microhardness of 522 $HV_{0.5/15}$ and 356 $HV_{0.5/15}$ on the AISI 431 and AISI 316L depositions. It was also found that the different characteristics of the addition metals, considering their morphology, particle size distribution, and flow rate, led to significant changes in the geometric features of the depositions.

1. Introduction

In many industrial applications, equipment and components may be exposed to aggressive operational conditions, such as elevated temperatures and pressures, corrosive media, and high mechanical loads (Ref 1). Given the very many industrial uses of such equipment and components, rigorous criteria are needed in the selection of materials that are durable under extreme conditions, in order to maintain reliability and safety during operation (Ref 1, 2).

It is essential to develop materials suitable for highly demanding applications, although this can increase the operational costs. Carbon steels are among the most widely used materials, especially considering their low costs. However, these steels have limitations, notably when they are exposed to extreme temperature fluctuations and corrosive environments (Ref 3, 4).

One way to reduce costs, while maintaining good mechanical properties of the material, is to apply a coating (Ref 4). The deposition of a surface coating can improve the physicochemical and mechanical properties of the material, consequently increasing the useful life of the component. The coating, which should have more noble characteristics, acts as a barrier protecting the substrate against conditions that could cause its deterioration (Ref 4, 5).

Many materials can be used as coatings, with stainless steels being suitable due to their superior mechanical and physicochemical properties, compared to carbon steels (Ref 4). In particular, austenitic and martensitic stainless steels are used where high performance is required (Ref 4, 6). Austenitic stainless steels are mostly used in components and equipment that need to be resistant to corrosion and oxidation at high temperature, such as in the chemical and petrochemical industries (Ref 4, 6-8). Martensitic stainless steels are indicated for situations where high resistance to wear, cavitation, and erosion is required, so they are used for components such as propellers, valves, engine shafts, and steam turbines (Ref 9-14).

E.W.A. Figueredo, L.H.R. Apolinario, M.V. Santos, and A.C.S. Silva, Department of Mechanical Engineering, Universidade Federal de Pernambuco, Av. da Arquitetura, s/n, Recife 50740-550, Brazil; and Brazilian Institute for Material Joining and Coating Technologies (INTM), Universidade Federal de Pernambuco, Recife, Brazil; J.A. Avila, São Paulo State University (UNESP), São João da Boa Vista, Brazil; M.S.F. Lima, Photonics Division, Department of Aerospace Science and Technology, Institute of Advanced Studies, São José dos Campos, Brazil; T.F.A. Santos, Department of Mechanical Engineering, Universidade Federal de Pernambuco, Av. da Arquitetura, s/n, Recife 50740-550, Brazil; Brazilian Institute for Material Joining and Coating Technologies (INTM), Universidade Federal de Pernambuco, Recife, Brazil; and Brazilian Northeast Aerospace Network, Universidade Federal de Pernambuco, Recife, Brazil. Contact e-mail: tiago.felipe@ufpe.br.

Laser cladding is a process involving fusion deposition of a thin layer of addition metal on the surface of a substrate, using a high power density laser beam as the heat source (Ref 12, 15, 16). Advantages of the laser cladding process, compared to competing processes, are that it can be used to produce complex components, offering high processing speed, high precision, potential for automation, and good repeatability. Despite a low thermal input, the technique provides a high energy density, while the heat-affected zone is small (Ref 6, 7, 15, 17-19). An important advantage of the process is the low dilution values that can be achieved. A dilution range of 10-20% for a single pass produces depositions with good metallurgical union, satisfactory mechanical properties, and acceptable corrosion resistance (Ref 9, 19-21). The characteristics of the depositions in laser welding processes are influenced by variables including wavelength, beam diameter, power density, laser scanning speed, electromagnetic transverse mode, physical properties of materials (such as reflectivity and thermal diffusion), the type and flow of shielding gas, and the plasma induced by the laser (Ref 18, 22). These factors influence the geometric, microstructural, mechanical, and physicochemical characteristics of depositions (Ref 4, 7, 10, 17). Although laser cladding is now widely used in industry, appropriate control of the various process variables is essential for the treatment of different materials. Furthermore, the different types of materials incorporated in production of the coatings require specific process conditions. Moradi et al.(Ref 13), Alvarez et al. (Ref 19), and Moradi et al. (Ref 10) detailed the influencing of both the laser parameters and the proprieties of the addiction metal powder on the geometry of the final depositions. Therefore, it is important to define the operational window of the process, with the fusion with the substrate being controlled in order to ensure depositions with no defects and good metallurgical bonding between the substrate and the coating (Ref 2, 15, 19, 20, 23).

In the present study were produced beads of AISI 431 and AISI 316L on an ASTM A-36 carbon steel substrate, varying both the laser power and scanning speed. The relations among geometric characteristics such as height, width, penetration, H/W ratio, dilution, and wettability angle were investigated, in order to understand the use of this technology in the processing of materials. Therefore, this manuscript contributes to the understanding and development of laser deposition processes suitable for achieving high-quality laser cladding coatings of AISI 431 and AISI 316L stainless steels on carbon steel substrates, considering important properties such as dilution, wettability, and coating overlap, which are influenced by the laser beam power input and scanning speed, which is a key point to produce coating. As we expected, the coating demands bead overlap; thus, producing large width bead with appropriate reinforcement is essential to make possible the good properties coatings by laser cladding.

2. Materials and Methods

The addition metals used for the laser cladding depositions were a martensitic stainless steel (AISI 431) and an austenitic stainless steel (AISI 316L). The two powdered materials are shown in Figure 1. The AISI 431 steel was manufactured using water atomization, resulting in particle sizes between 69 and 101 μm. The AISI 316L steel was manufactured using gas atomization, with particle sizes from 45 to 106 μm. It can be seen from Figure 1 that the particles produced by atomization using water were more homogeneous than those atomized using gas, presenting spherical shapes with small satellite particles. The substrate employed was ASTM A-36 carbon steel, in the form of a plate with thickness of 6.35 mm. Table 1 shows the chemical compositions of the materials used in this work.

The samples were produced using a disk laser (TruDisk 6002, Thumpf Inc.) with maximum power of 6000 W, beam quality of 8 mm-mrad, wavelength of 1030 nm, and fiber diameter of 200 μm. The movement system consisted of a high precision robot (Model KR 60 HA, KUKA) and a disk metal feeding system (Model PF21-GTV). The laser head, produced by Fraunhofer Institute Laser Technology (ILT) with integrated autofocus, allows the autofocus determination automatically and with accuracy, in order to, the focus distance was maintained constant of 25 mm above the plane. The laser defocusing was carried out to obtain a conduction mode melting (Ref 24, 25), regularly intended in laser cladding process. The powder feeder had a disk with a groove 5 mm wide and 0.6 mm deep, with the feed delivery being constant and directly proportional to the disk rotation speed. The coaxial feeding occurred through the laser head axially to the laser beam through the direct metal deposition technic (Ref 13, 14).

The process parameters were selected considering their influence on the coating, based on a review of the literature, where the main authors consulted were Sharifitabar and Halvee (Ref 11), Goodarzi et al. (Ref 26), Moradi et al. (Ref 10), Sun et al. (Ref 17), and Apolinario et al. (Ref 7). These studies indicated that the laser beam power and scanning speed were among the parameters with greatest influence on the final characteristics of the depositions produced by the laser cladding process. Therefore, these were the central parameters considered during production of the samples.

In preliminary tests, the input parameters varied were the laser beam power (P) and scanning speed (v), as shown in Table 2. For both addition metals, the other laser parameters were kept constant throughout the process, as follows: focal length of 25 mm, zero incidence angle, argon shielding gas, ~3.2 mm focus diameter, carrier gas flow rate of 7 SLPM, and disk rotation speed of 10 rpm.

It should be noted that for the AISI 316L addition metal, the depositions were initially produced using the same values for the power (800, 1000, 1400, and 1600 W) and scanning speed (9, 14, and 16 mm/s) as employed for the AISI 431 addition metal. However, preliminary analyses of the cross sections of these depositions showed that there was no significant union zone. Therefore, the power values were increased to 1900, 2100, 2400, and 2600 W, in order to obtain acceptable dilution values.

For both addition metals, the powder flow rate was determined as the average of five measurements of the amount of powder (in g) injected over a period of 2 min, using a carrier gas flow rate of 7 SLPM (standard liters per minute) and disk rotation speeds of 1, 3, 6, 8, and 10 RPM. The aim of these measurements was to quantify the addition metal powder flows during the deposition process, since differences in particle size distribution and morphology influence the powder flow rate, consequently affecting the final characteristics of depositions.

For metallographic analysis, the samples were cut transversely and embedded in bakelite, followed by preparation using sandpaper (180-1500 mesh) and polishing with diamond pastes (3 and 1 μm particle sizes).
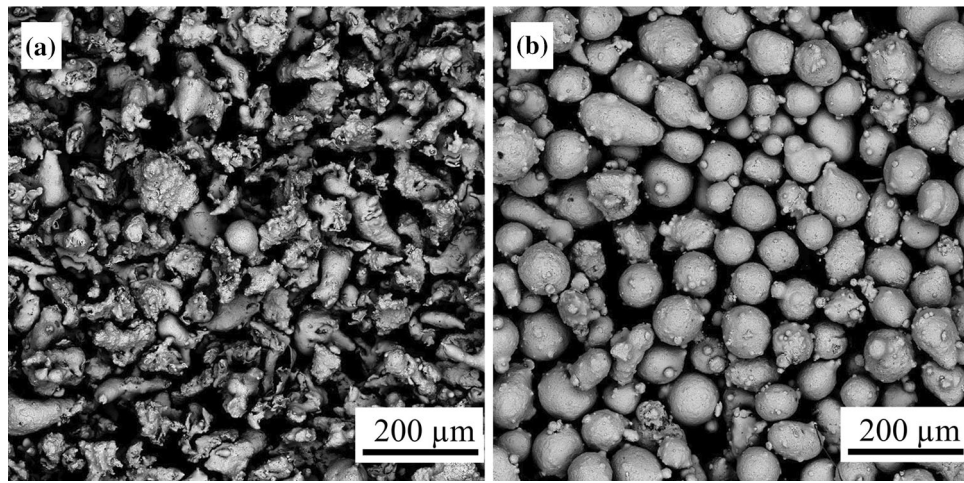
Fig. 1. Scanning electron micrographs of the AISI 341 (a) and AISI 316L (b) stainless steels

Table 1. Chemical compositions of the base metal and the powdered addition metals

Wt. Pct., %	C	Cr	Mn	Mo	N	Ni	O	P	S	Si	Fe
316L	0.01	16.24	1.09	2.42	0.05	12.37	0.04	0.04	0.01	0.50	Bal.
431	0.17	16.5	0.1	…	…	1.97	…	0.01	0.01	0.7	Bal.
A-36	0.12	0.05	0.78	0.01	…	0.06	…	0.02	0.012	0.11	Bal.

Table 2. Experimental configurations for depositions of the AISI 431 and AISI 316L stainless steels

Condition	P, W	v, mm/s	Cladding material	Condition	P, W	v, mm/s	Cladding material
1	800	9	AISI 431 and AISI 316L	13	1900	9	AISI 316L
2		14		14		14	
3		16		15		16	
4	1000	9		16	2100	9	
5		14		17		14	
6		16		18		16	
7	1400	9		19	2400	9	
8		14		20		14	
9		16		21		16	
10	1600	9		22	2600	9	
11		14		23		14	
12		16		24		16	

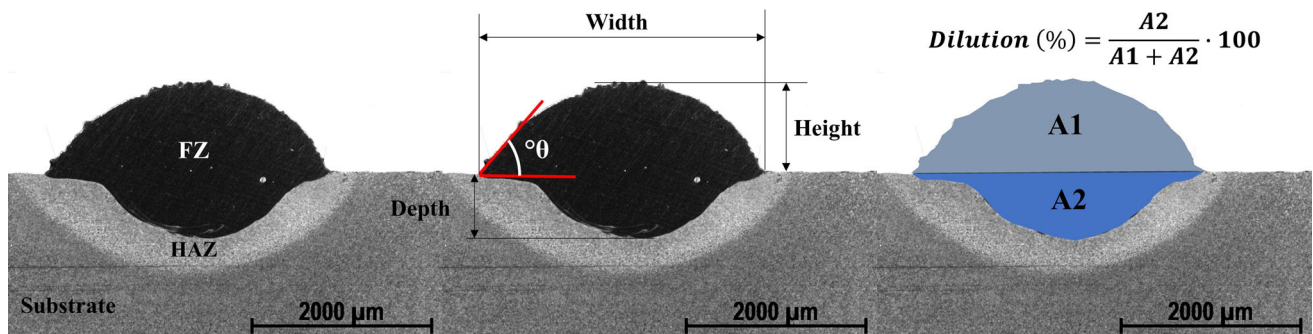$$Dilution\ (\%) = \frac{A2}{A1 + A2} \cdot 100$$

Fig. 2. Illustrative cross sections of the weld deposition: (a) macro-regions including the fusion zone (FZ), heat-affected zone (HAZ), and substrate; (b) depth, width, and height measurements; and (c) the regions used for the dilution calculation

The geometric characteristics, H/W ratios, dilution values, and wettability angles were obtained from the images of the depositions, employing ImageJ software. Figure 2 shows a schematic illustration of the deposition cross section, indicating the calculated geometric characteristics. The H/W ratio indicates the degree of convexity of the bead, calculated as the ratio between the height of the reinforcement and the width of the bead. The dilution is the portion of the base metal/substrate in the mixture with the addition metal, measured by the geometric method using the quotient between the area of the deposition below the substrate surface line (A2) and the total bead area (A1 + A2). The wettability is the angle (°θ) between the substrate line and the surface of the bead.

Quantification of hardness employed the Vickers hardness test, using an Emcotest DuraScan G5 microhardness meter with a load of 500 g, load time of 15 s, and distance of 0.25 mm between indentations, performed on the cross section of the specimen. The results were obtained as the mean of three measurements, mapping the hardness profile in the different deposition regions (fusion zone, heat-affected zone, and substrate).

All the conditions were evaluated considering four parameters: dilution, geometric characteristics, bead wettability, and presence of defects. The analyses identified depositions meeting the required production criteria, in addition to providing an assessment of the influence of the parameters on the deposition characteristics.

3. Results and Discussion

3.1 Characterization of the Depositions

Macrographs and micrographs of the cross sections of the samples produced using the AISI 431 and AISI 316L stainless steels were used for the evaluation of dilution, geometric characteristics, wettability, and presence of defects.

Tables 3 and 4 provide the geometric characteristics of the depositions for each condition shown in Table 2, together with the values for the H/W ratio, wettability, power density (PD), and laser beam interaction time (t_i), which is illustrated in Eq 1; D and v represent the incident beam length and the laser scanning speed, respectively (Ref 27). From analysis of the cross sections, it could be concluded that the laser beam power and scanning speed had a combined influence on the height,

width, penetration, fusion zone, and wettability of the depositions.

$$t_i = \frac{D}{V} \qquad \text{(Eq 1)}$$

Figure 3 and 4 shows macrographs of the cross sections of the depositions of the AISI 431 and AISI 316L stainless steels, respectively, produced using different processing parameters. It can be visually seen that the geometric characteristics of the depositions were modified by varying the laser beam power and scanning speed. The depositions presented zones of mixing with the substrate, with the fusion zone increasing with increase in the laser power. It can also be seen that the height of the deposition decreased with the increase in the scanning speed. It is important to mention that the effects of the laser beam power and scanning speed on the geometric characteristics of the depositions were similar for the two addition metals.

As shown in Figure 5, the depositions of both addition metals were homogeneous, crack-free, and with roughness caused by the process. Irrespective of the addition metal used, the scanning electron micrographs of the deposition surfaces showed attached solid particles and empty spaces, resulting in a rough surface. The shapes of the particles trapped on the surface were characteristic of the addition metal powder, indicating that some particles that had not melted were adhered to the surface during the deposition process. This could be attributed to the high powder flow and/or insufficient power density to melt all the particles introduced during the process, as also noted by Shah et al. (Ref 28).

For both depositions, the cross sections showed the presence of dispersed pores (Figure 6), possibly caused by gases that were trapped in the material during solidification of the melt pool, due to insufficient time for their escape. A characteristic of materials submitted to laser processing is that a high speed of the solidification front favors the trapping of gases in the melt pool. The gases are produced during the fusion process from contaminants present in the materials or from vaporization of the addition metal and the substrate, as also observed by Miranda et al. (Ref 29) and Sun et al. (Ref 17).

The depositions of AISI 431 stainless steel presented greater quantities of pores, compared to the AISI 316L depositions, which could be attributed to the gases generated during the fusion process, as well as the irregular morphology of the AISI 431 addition metal particles. In previous studies, Pajukoski et al.(Ref 30) and Aubry et al. (Ref 18) found that the powder

Table 3. Geometric characteristics of the depositions using AISI 431 stainless steel

Condition	P, W	v, mm/s	Height, mm	Width, mm	Depth, mm	H/W	Wettability, °θ	t_i, s	PD, W/mm^2
1	800	9	0.71	2.28	0.028	0.31	50.47	0.27	176.84
2		14	0.41	1.91	0.010	0.21	27.84	0.17	
3		16	0.23	1.89	0.005	0.12	32.10	0.15	
4	1000	9	0.63	2.20	0.019	0.28	68.08	0.27	221.05
5		14	0.50	2.13	0.020	0.23	48.77	0.17	
6		16	0.39	1.71	0.020	0.22	45.69	0.15	
7	1400	9	0.74	2.84	0.072	0.26	59.25	0.27	309.47
8		14	0.54	2.71	0.070	0.20	45.15	0.17	
9		16	0.42	2.63	0.110	0.16	32.45	0.15	
10	1600	9	0.85	2.93	0.081	0.29	63.05	0.27	353.68
11		14	0.5	2.84	0.140	0.18	25.24	0.17	
12		16	0.47	2.81	0.130	0.17	35.63	0.15	

Table 4. Geometric characteristics of the depositions using AISI 316L stainless steel

| Condition	P, W	v, mm/s	Height, mm	Width, mm	Depth, mm	H/W	Wettability, °θ	t_i, s	PD, W/mm²
1	800	9	1.03	1.87	0.014	0.55	91.89	0.27	176.84
2		14	0.77	1.11	0.011	0.69	71.85	0.17	
3		16	0.60	1.03	0.017	0.58	65.44	0.15	
4	1000	9	1.29	1.75	0.023	0.74	106.64	0.27	221.05
5		14	0.79	1.90	0.008	0.42	69.57	0.17	
6		16	0.72	2.11	0.012	0.34	57.88	0.15	
7	1400	9	1.31	2.33	0.024	0.56	102.54	0.27	309.47
8		14	0.88	2.37	0.032	0.37	78.69	0.17	
9		16	0.76	2.37	0.014	0.32	63.82	0.15	
10	1600	9	1.45	2.62	0.033	0.55	113.14	0.27	353.68
11		14	0.94	2.50	0.055	0.38	69.82	0.17	
12		16	0.81	2.46	0.018	0.33	55.42	0.15	
13	1900	9	1.41	3.01	0.081	0.47	79.47	0.27	419.99
14		14	1.00	2.85	0.197	0.35	65.41	0.17	
15		16	0.84	2.78	0.212	0.30	60.03	0.15	
16	2100	9	1.39	3.37	0.303	0.41	73.50	0.27	464.20
17		14	0.89	3.15	0.292	0.28	60.46	0.17	
18		16	0.82	3.00	0.386	0.27	55.31	0.15	
19	2400	9	1.43	3.39	0.469	0.42	70.31	0.27	530.52
20		14	0.97	3.12	0.715	0.31	62.25	0.17	
21		16	0.81	3.07	0.549	0.26	55.93	0.15	
22	2600	9	1.40	3.35	0.815	0.42	78.08	0.27	574.73
23		14	0.96	3.15	0.705	0.31	60.23	0.17	
24		16	0.81	3.10	0.662	0.26	45.94	0.15	
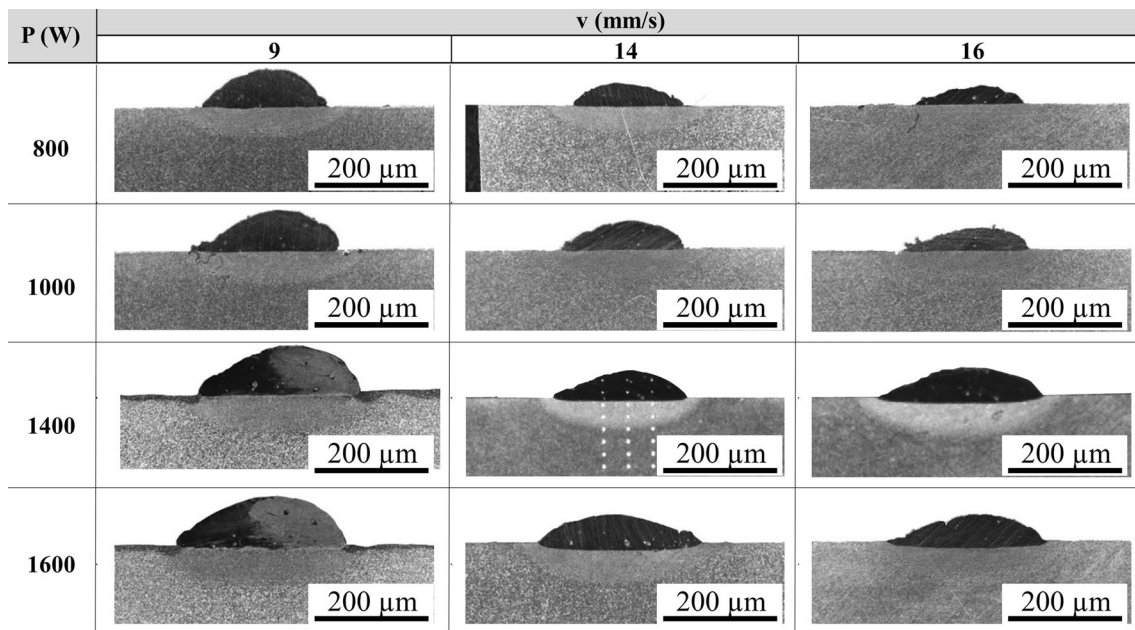
Fig. 3. Cross sections of the depositions using AISI 431 stainless steel

quality and production method influenced the creation of defects during the deposition process, with such defects being reduced when the particles were spherical and uniform. Benedetti et al. (Ref 31) reported that spherical particle morphology led to greater coalescence between the particles, compared to irregular morphologies, with better interaction during energy transfer leading to lower pore creation. Riabov and Bengtsson (Ref 32) related the lower porosity in beads produced with gas-atomized powder to the lower oxides quantities on these particles, compared to water process. In contrast to the water atomization, gas atomization process carries out in vacuum or under an inert atmosphere in order to protect elements being oxidized (Ref 33).

3.2 Influence of Laser Power on Deposition Geometry

For both materials, the laser power influenced the height and width of the depositions (Figure 7), as reported previously by Liu et al. (Ref 2), Nabhani et al. (Ref 15), Aghili and
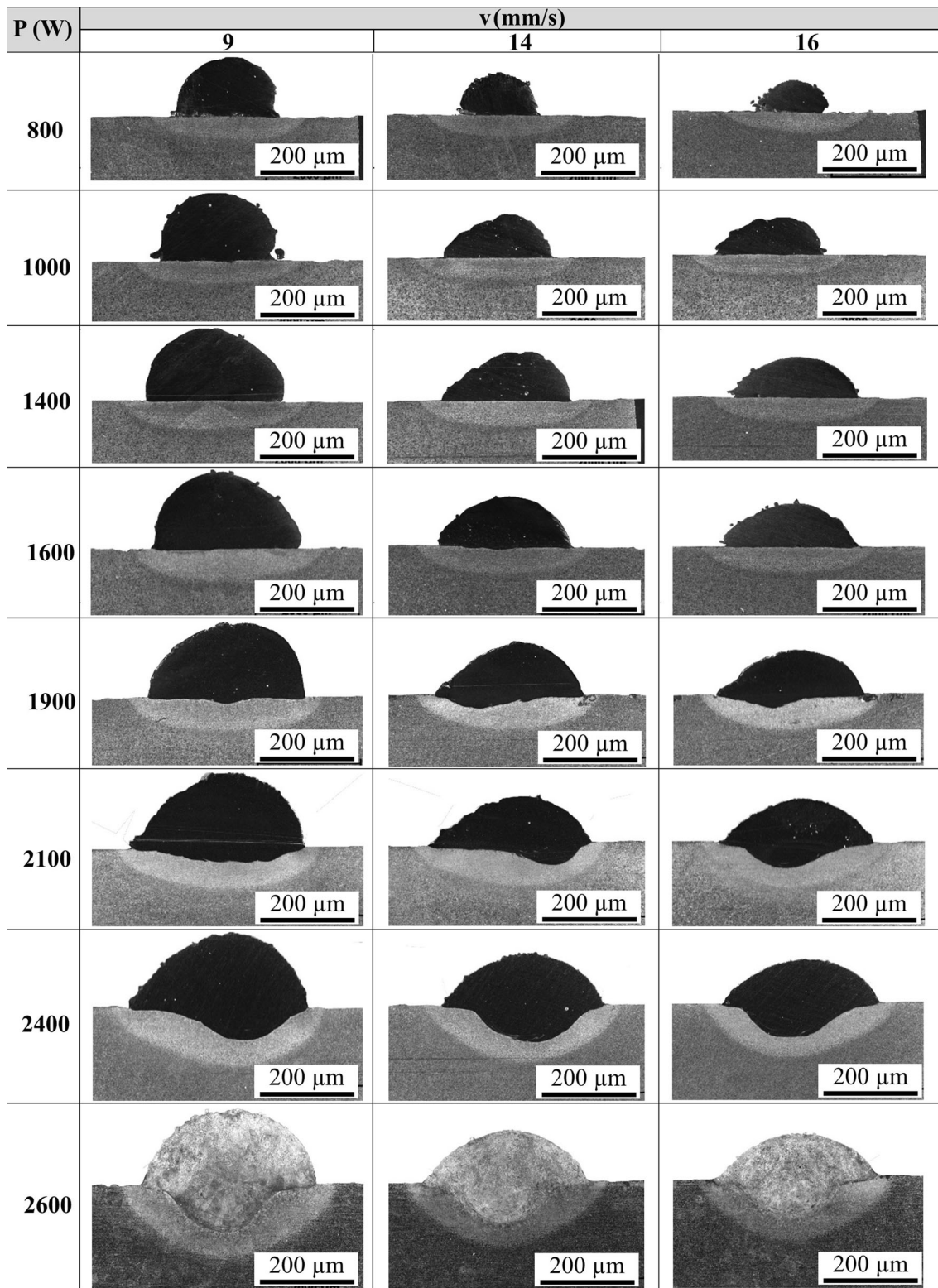
Fig. 4. Cross sections of the depositions using AISI 316L stainless steel

Shamanian (Ref 23), El Cheikh et al. (Ref 34), Zhong et al. (Ref 35), and Corbin et al. (Ref 36). For example, using a laser beam scanning speed of 16 mm/s, increase of the power from 1000 to 1400 W resulted in the AISI 431 deposition height and width increasing from 0.39 and 1.71 mm to 0.42 and 2.63 mm,

respectively. For AISI 316L, the values increased from 0.72 and 2.11 mm (1000 W) to 0.76 and 2.37 mm (1400 W).

For the same laser beam scanning speed, increase of the power led to moderate increases of the deposition heights. This was due to the higher energy density directed toward fusion of the addition metal and the substrate, which resulted in a greater
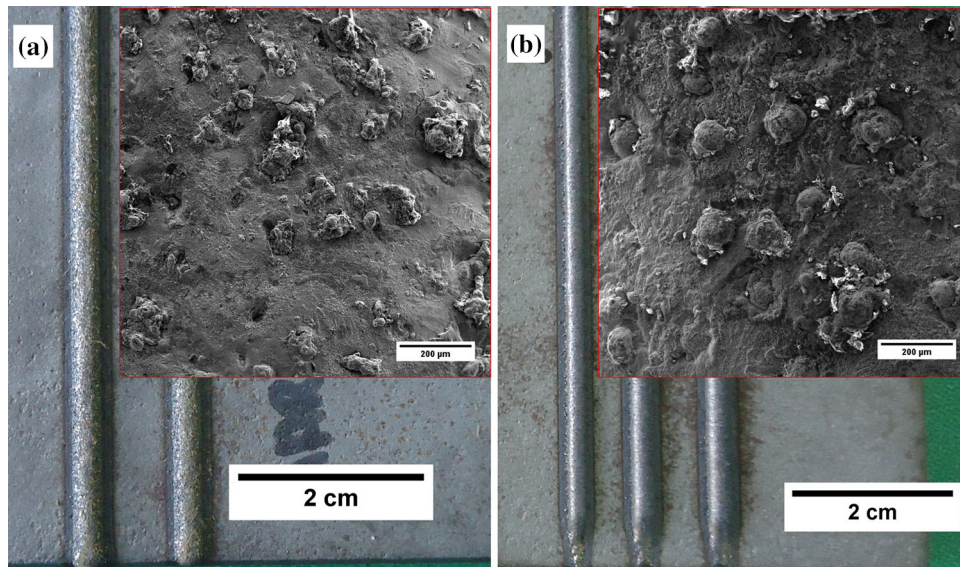
Fig. 5. Scanning electron micrographs of the depositions obtained using the AISI 341 (a) and AISI 316L (b) stainless steels. The higher magnifications show the top surfaces of the depositions
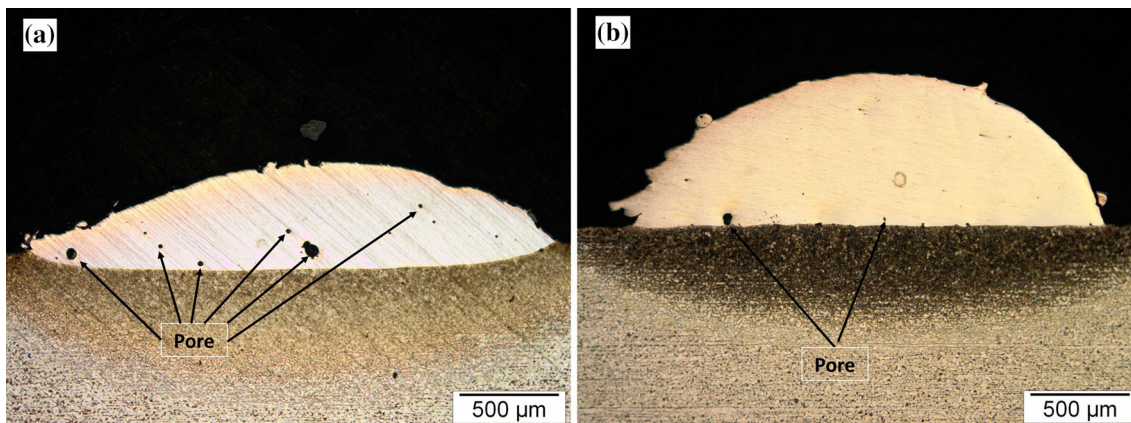
Fig. 6. Cross sections showing the presence of pores: (a) AISI 431 and (b) AISI 316L

amount of fused powder and, consequently, a deeper deposition.

The laser power had a greater influence on the widths of the depositions, as can be seen from Figure 7 and the values in Table 3 and 4. This could be attributed to the Marangoni forces, which have the greatest influence on the heat distribution in the melt pool (Ref 12, 15, 22). Marangoni forces arise from the surface tension difference due to the temperature variation between the center of the melt pool and the adjacent regions, creating a convective flow (the Marangoni effect) from the center to the sides. This results in greater heat transfer to the extremities of the melt pool, hence increasing the deposition width.

3.3 Influence of Laser Beam Scanning Speed on Deposition Geometry

Figure 8 shows the behaviors of the heights and widths of the depositions, according to variation of the laser beam scanning speed. For both materials, it can be seen that a faster scanning speed reduced the heights and widths of the depositions (Tables 3 and 4). A faster speed also decreased

the H/W ratio, with the depositions presenting a lower degree of convexity, implying better wettability. Previous studies have recommended a wettability angle of less than 80° for single-pass depositions, since this reduces the possibility of subsequent pore formation and lack of fusion between passes, optimizing the metallurgical union between the coated layers (Ref 12, 36, 37). The results showed that the deposition height was influenced to a greater extent by variation of the laser beam scanning speed, while the width showed a greater influence of the laser beam power, in agreement with the findings discussed in the previous section.

The reduced widths and (especially) the heights of the depositions with increase of the scanning speed were due to the smaller volume of addition metal deposited per unit area, together with a shorter interaction time (Eq.1) and, consequently, a smaller amount of energy. Hence, increase of the speed resulted in a shorter residence time over a particular area, reducing the amount of addition metal introduced, so a smaller amount of material was melted to produce the deposition. The effects of a faster laser beam scanning speed on decreasing the deposition height and width, while increasing the wettability,
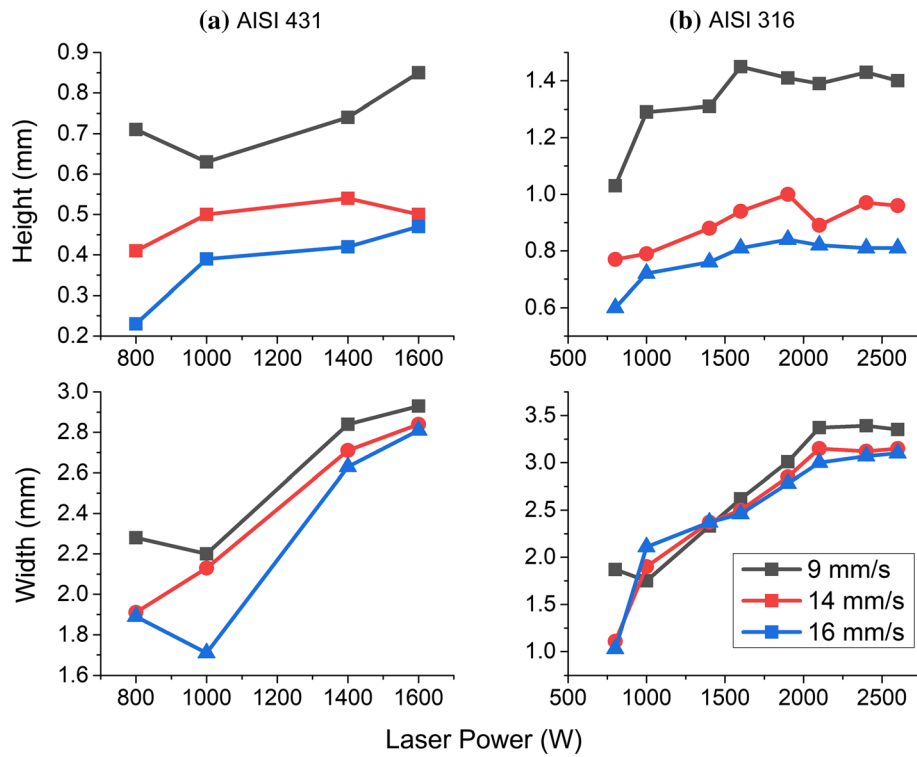
Fig. 7. Influence of laser beam power on deposition height and width using (a) AISI 431 and (b) AISI 316L
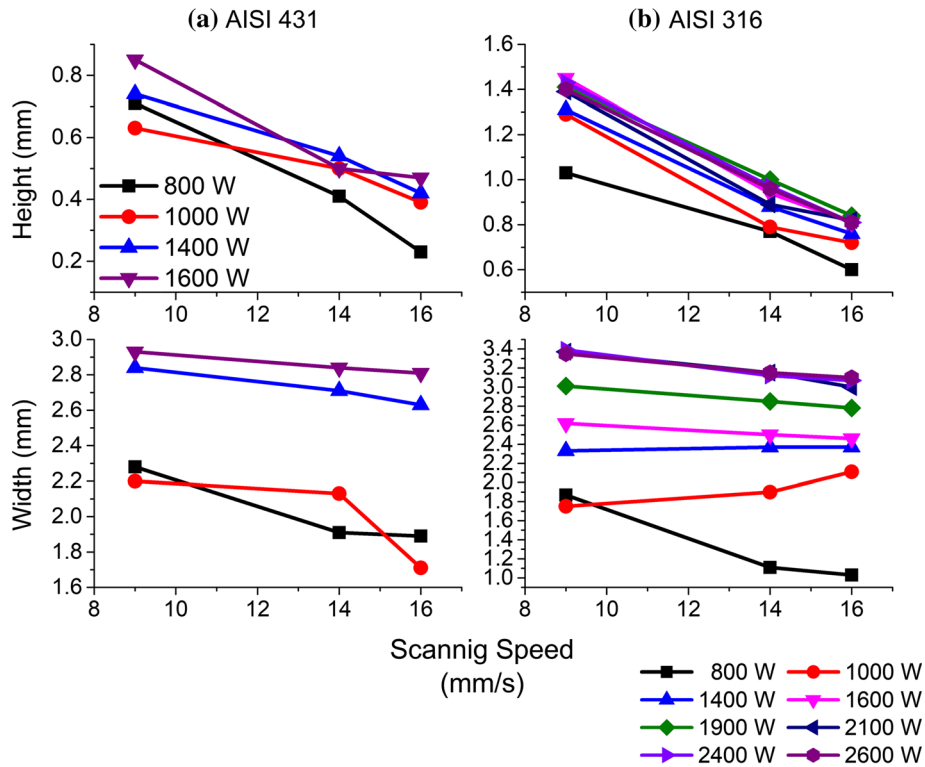

Fig. 8. Effect of laser beam scanning speed on deposition height and width using (a) AISI 431 and (b) AISI 316L

have also been reported by El Cheikh et al. (Ref 34), Zhong et al. (Ref 35), Corbin et al. (Ref 36), Nabhani et al. (Ref 15), Aghili and Shamanian (Ref 23), Apolinario et al. (Ref 7), Liu et al. (Ref 2), and Alvarez et al. (Ref 19).

3.4 Influence of Laser Beam Power and Scanning Speed on Dilution

Figure 9 shows the dilution values for the depositions produced using the two addition metals. For the depositions of
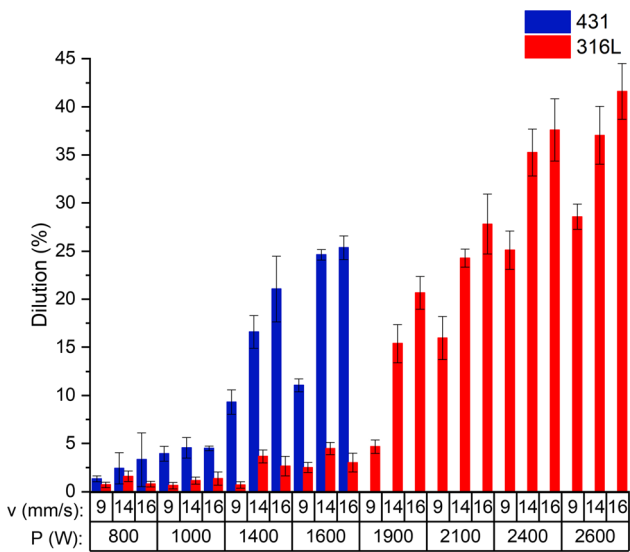
Fig. 9. Results of the dilution calculations for the AISI 431 and AISI 316L stainless steel depositions

AISI 431, using power values of 1400 and 1600 W, increase of the scanning speed, with shorter interaction between the beam laser and the material surface, led to significantly greater dilution. When power values of 800 and 1000 W were used to produce the depositions, alteration of the speed did not significantly change the dilution.

In the case of the AISI 316L depositions, the effect of scanning speed on dilution was not significant for power values up to 1600 W. The effect of a faster speed on dilution was only observed for power values between 1900 and 2600 W, where a faster speed led to a moderate increase of dilution.

It should be noted that the effect of greater dilution with change of the laser beam scanning speed was only observed for the samples processed using the highest power values (which delivered the highest power densities). In addition, it was evident that the influence of scanning speed on dilution occurred in different power ranges for the two materials employed, which could be attributed to the different powder flows, surface tensions, particle sizes, and morphologies of the materials.

Increase of the scanning speed may reduce dilution, since the amount of energy transferred to the substrate is lower at higher speed, so the dilution zone becomes smaller. However, increased dilution at higher speed has also been reported in studies of laser cladding and laser welding (Ref 7, 22, 34, 35).

The direct relation observed between scanning speed and dilution could be explained by reduced efficiency of absorption of the laser beam energy by the plasma (plasma shielding), when the scanning speed was increased, which would allow greater energy transfer from the laser beam for melting of the substrate, consequently leading to higher dilution values. This mechanism has been mentioned previously by Aguilera et al. (Ref 38), Vadillo et al. (Ref 39), Katayama et al., (Ref 22), Apolinario et al. (Ref 7), and Xu et al. (Ref 40).

However, Katayama et al. (Ref 22) reported that the effect of the absorption of energy from the laser beam by the plasma was only significant for a laser beam with longer wavelength, which is not applicable for a disk laser such as the one used in the present study. Hence, it is not possible to attribute an increase

of dilution with increase of the scanning speed to reduction of the plasma shielding effect.

In a process with directed energy, using coaxial injection of the addition metal, the laser beam is incident on the focal point of the powder flow. However, increase of the laser beam scanning speed leads to a condition where the focal point of the laser no longer coincides with the focal point of the powder, because the mass of powder is retarded by the effect of inertia. Hence, the increased dilution with increased scanning speed could be explained by the difference in the distance between the focal point of the laser beam and the focal point of the powder flow. Accordingly, a greater quantity of laser beam energy was directed at the substrate, producing depositions with higher dilution values, as the scanning speed was increased. This also led to reductions of the width and (especially) the height of the depositions.

Evaluation of the effect of the laser power showed that for power values of 800 and 1000 W, dilutions lower than 5% were obtained for the depositions of AISI 431 stainless steel, at all laser beam scanning speeds. This could be explained by the low power density imposed during formation of the deposition, which was insufficient to generate a satisfactory fusion zone of the addition metal and the substrate. However, power values of 1400 and 1600 W led to acceptable dilutions of between 9.3 and 25.4%, due to the higher imposed power density. Furthermore, the depositions produced using power values of 1400 and 1600 W presented better wettability, compared to the depositions produced using powers of 800 and 1000 W (Table 3). It could also be seen that for 800 and 1000 W (with lower power densities), increase in the scanning speed led to no significant increase in dilution. Increased dilution was only observed for powers of 1400 and 1600 W.

The depositions of AISI 316L stainless steel required the use of higher power values to achieve adequate dilution, since powers between 800 and 1600 W resulted in depositions with dilutions lower than 5%. The use of powers of 1900, 2100, 2400, and 2600 W resulted in depositions with dilutions from 15.4 to 41.6%. Analogously to the AISI 431 depositions, increase in the power led to higher dilution, while increase in the laser beam scanning speed also resulted in higher dilution for power values above 1900 W. It should be noted that some depositions showed excessively high dilution values of between 30 and 41%. These high values observed at the highest powers could alter the physicochemical and mechanical properties of the coating and the substrate, as reported by Da Luz et al. (Ref 4), Zhong et al. (Ref 20), and Goodarzi et al. (Ref 26).

Nevertheless, Pajukoski et al. (Ref 30) found that when depositions with excessive dilutions of around 30 to 44% were used for the production of continuous coatings with an overlap rate of between 50 and 60%, the overall dilution for the coating decreased to around 6.5%. The reduction of dilution with the formation of overlapping can be explained by the fact that part of the laser energy is used for a second fusion of part of the adjacent material deposited previously. Nabhani et al. (Ref 15), Costa et al. (Ref 41), and Ansari et al. (Ref 37) recommended that for single-pass depositions, the dilution should be between 15 and 25%, in order to ensure perfectly bonded coatings after overlapping of the beads. It was also reported that coatings with 5-10% dilution presented perfect metallurgical bonding between the materials after laser processing. These findings suggest that it is advisable to study the effect of variation of the overlap on dilution, while taking into account that reduction of dilution also depends on several other factors, including the

power setting, laser beam scanning speed, and powder flow rate, as well as the type of material used and the particle size and morphology.

The results indicated that for both materials, increase in the laser power led to higher dilution and improved wettability of the depositions. Similar behavior was observed in previous studies by Zhong et al. (Ref 35), Pajukoski et al. (Ref 30), Näkki et al. (Ref 21), Nabhani et al. (Ref 15), Aghili and Shamanian (Ref 23), and Apolinario et al. (Ref 7). Higher dilution values were closely related to increase of the laser power and, consequently, higher power density. The findings demonstrated that the laser power was the parameter that had the greatest effect in increasing the dilution, in agreement with Nabhani et al. (Ref 15) and Aghili and Shamanian (Ref 23).

The laser power determines the amount of energy (energy density) directed toward fusion of the materials to be joined. Therefore, control of the laser power is essential in the production of coatings, because power outside the operational window of the process can cause either excessive fusion or absence of metallurgical union of the materials. As discussed previously, high power values can cause high dilutions that may negatively affect the properties of the materials, favoring the emergence of defects such as cavities, transient holes, and poor homogeneity of the fusion zone. On the other hand, low power values can cause lack of fusion, low or no metallurgical union of the materials, and greater wastage of the addition metal.

Figure 10 shows cross sections of AISI 316L depositions obtained under different conditions. For depositions produced using higher power values, there was non-uniformity of the fusion zone across the width of the bead. Non-uniformity of the fusion zone results from excessive fusion at the center or at the extremities of the deposition. This type of asymmetry has also been described by Goodarzi et al. (Ref 26), Pajukoski et al. (Ref 30), Pekkarinen et al. (Ref 42), and Näkki et al. (Ref 21).

According to Goodarzi et al. (Ref 26), asymmetry of the deposition fusion zone mainly occurs due to modification of the Gaussian distribution of the laser beam energy with increase of the power, or to the injection of a non-homogeneous powder flow in the regions subjected to the laser beam. In the present work, it was not possible to confirm a change in the Gaussian distribution of the laser beam energy, since this is not a trivial task. Nonetheless, the findings indicated that this occurred at the highest power values.

Considering the powder flow, it is possible that there may have been a non-homogeneous injection of the addition metal, which could have led to asymmetry of the deposition fusion zones. A non-homogeneous powder flow could be caused by blockage or reduction of the powder flow in the addition of metal delivery tubes in the head. This would act to reduce the amount of powder in a particular deposition region, favoring asymmetry of the fusion zone.

3.5 Comparison of the Depositions Obtained Using the AISI 431 and AISI 316L Addition Metals

As shown in Table 3 and 4, the use of laser powers of 800, 1000, 1400, and 1600 W, with scanning speeds of 9, 14, and 16 mm/s, resulted in depositions with geometric characteristics that differed for the two addition metals. The depositions of AISI 316L stainless steel were higher, with higher H/W ratios and wetting angles, compared to the values obtained for the depositions of AISI 431 stainless steel. In addition, the dilution values (Figure 9) for the AISI 431 depositions were up to 25%, while those for the AISI 316L depositions were below 5%.

Moradi et al. (Ref 10) pointed out on their work that the physical proprieties of the materials influence on the geometric characteristics of the beads. De Oliveira et al. (Ref 43) indicated that both energy from laser beam and the one from the powder particles heated influences on the geometry of the deposition; in other words, particles that reach the metal pool with higher temperature favor higher value of width and lower of height. Based on Bonnet et al. (Ref 44) and the Online Materials Information Resource (www.matweb.com) (Ref 45), the austenitic stainless steel (316L) has higher value of specific heat than the martensite one. Therefore, it is reasonable to affirm that the powder AISI 431 reached the melt pool with higher temperature, which contributed to a higher and lower values of width and height, respectively, for the depositions. On the other hand, Näkki et al. (Ref 21) noted that for directed energy deposition processes, such as laser cladding, the nature of the powder plays a fundamental role in determining the final properties of the products. The differences found for depositions are associated with factors including the chemical composition, physical properties, particle morphology, size distribution, and flow rate of the addition metal.

Figure 11 shows a comparison of the particle size distributions of the addition metals. The AISI 316L powder presented a higher average particle size ($d_{0.5}$), compared to the AISI 431 powder, with values of 101.76 and 95.77 μm, respectively. The AISI 431 powder showed a higher percentage of larger particles, compared to the AISI 316L powder (Figure 11a), as well as greater
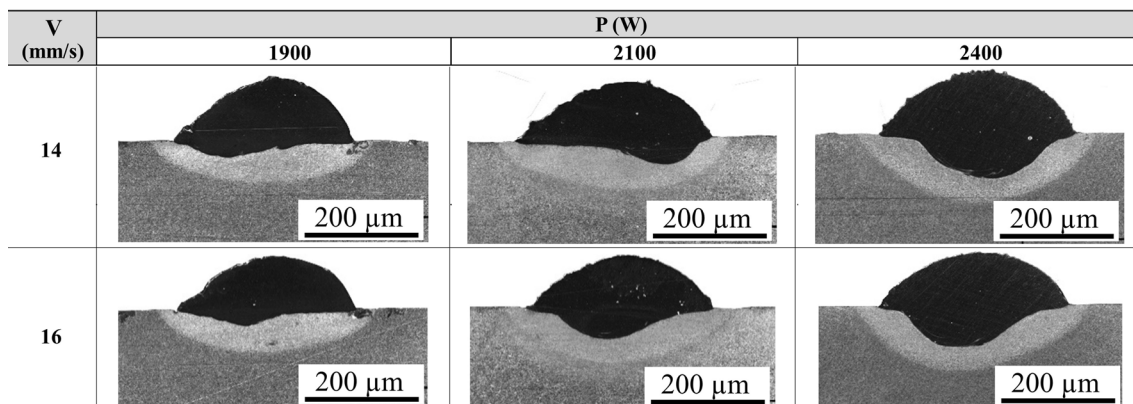
V	P (W)		
(mm/s)	1900	2100	2400
14	200 μm	200 μm	200 μm
16	200 μm	200 μm	200 μm

Fig. 10. Asymmetric fusion zones observed for the depositions of AISI 316L stainless steel
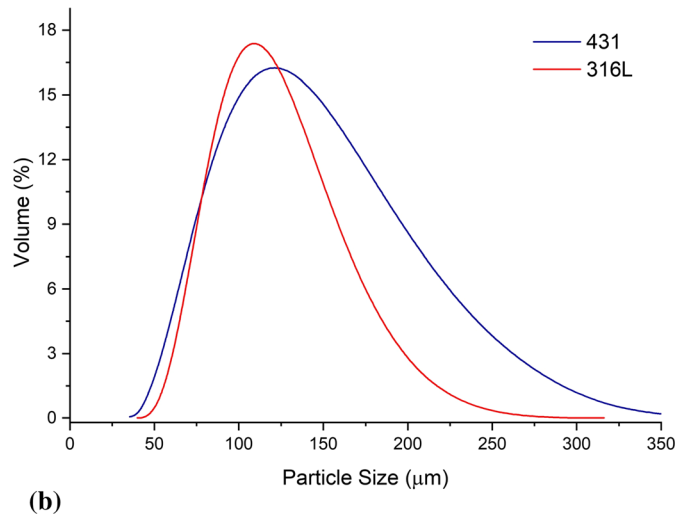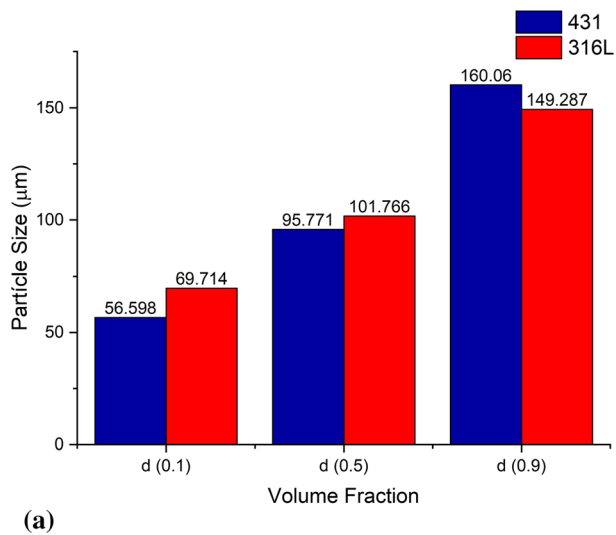
Fig. 11. (a) Particle size distributions of the powders and (b) asymmetric particle size distribution curves
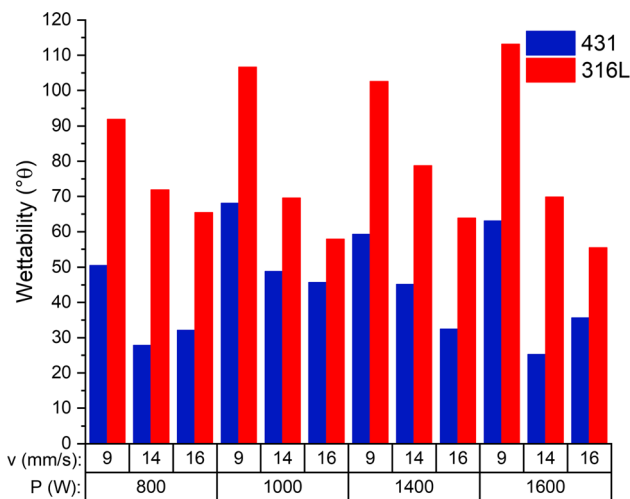

Fig. 12. Comparison of wettability values for the AISI 431 and AISI 316L stainless steel depositions

Fig. 13. Flow rates of the AISI 316L and AISI 431 addition metal powders, according to disk rotation speed

variability of particle size, as shown by the asymmetric size distribution curves (Figure 11b). It could be concluded that the geometric profiles of the depositions were influenced by both the particle size distribution and the powder flow rate.

The larger average particle size of the AISI 316L addition metal led to depositions with greater height and lower dilution, because larger particles require a greater quantity of energy to be completely melted for inclusion in the fusion zone. In other words, part of the energy that would be directed toward fusion of the substrate would be used to melt these particles.

Figure 12 shows the wettability angles for the depositions of the two materials, indicating that better wettability was obtained for AISI 431, which could be attributed to the smaller particle size of the AISI 431 addition metal. In the data on the wettability angles of the depositions, a tendency with the variation of the scanning speed or with the laser power for the AISI 431 stainless steel was not verified. On the other hand, for the deposition of the AISI 316L stainless steel, the reduction of the wettability angle was observed with increasing the speed to power values of 800, 1000, 1400, and 1600W. This reduction is also linked to the
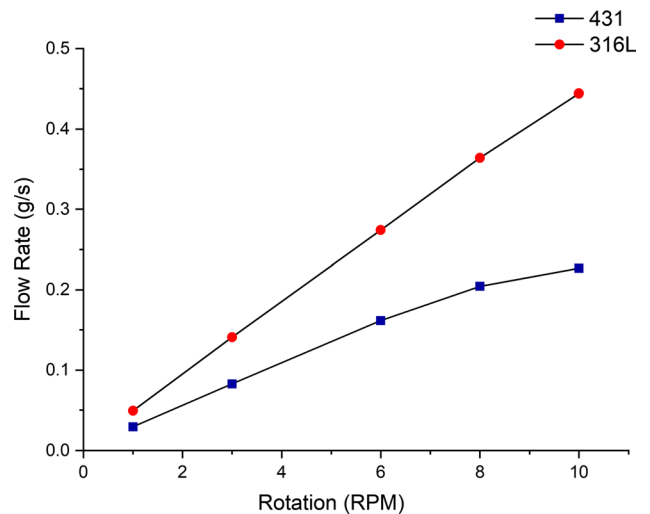
shorter nozzle residence time on the deposition region, which influenced the amount of material that was deposited. Tanigawa et al. (Ref 46) also found that the wettability of beads improved when the particle size was reduced.

The powder flow rate is another variable that directly influences the geometric characteristics of the deposition. Figure 13 shows the powder flow rates obtained with variation of the disk rotation speed. For the depositions produced in this study, all the conditions (for both addition metals) employed the same disk, the same rotation speed, and the same carrier gas flow, so these parameters should not have affected the powder flow rates of the two addition metal powders. However, the two powders presented different particle size and morphology, which would be expected to influence the amount of powder passing through the head and being added to the process. In order to confirm this, measurements were taken of the amounts of powder injected during a certain time at a given rotation speed. It was found that the flow rate of the AISI 316L powder was much higher than that of the AISI 431 powder, with values of 0.44 and 0.23 g/s, respectively.
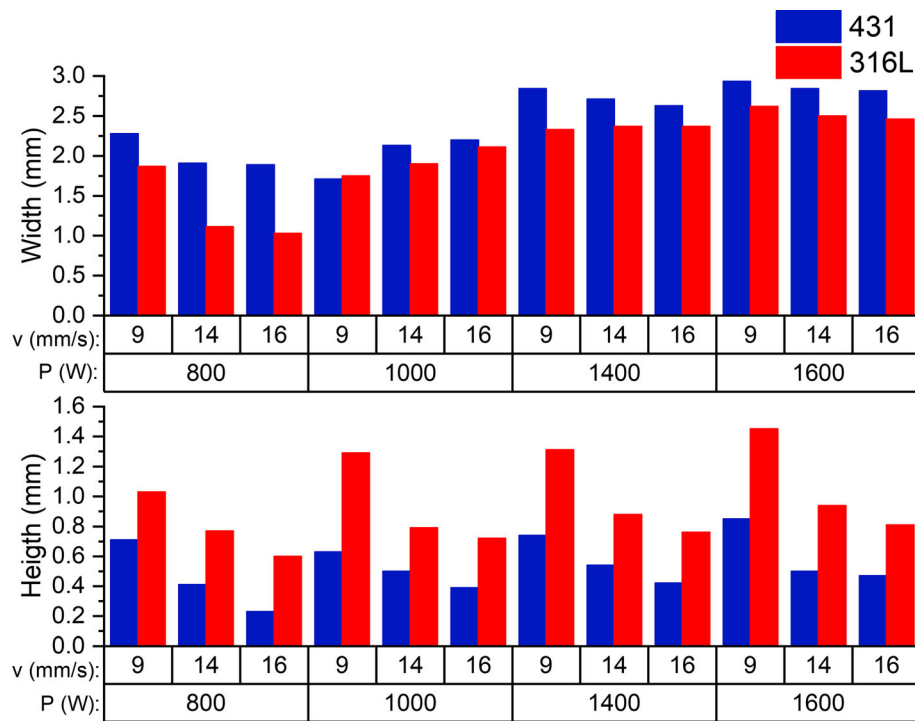
Fig. 14. Comparison of the heights and widths of the AISI 431 and AISI 316L stainless steel depositions

The size distribution analysis showed that the d(0.9) value (considering 90% of the particles) was smaller for the AISI 316L powder than for the AISI 431 powder, leading to a greater quantity of particles stored in the disk and transferred by the carrier gas, in agreement with the different calculated powder flow rates.

The greater quantity of powder injected in the AISI 316L deposition process resulted in higher depositions, lower width and dilution values, and low wettability. Shah et al. (Ref 28) reported that negative correlation between the powder flow rate and the fusion zone could be explained by the fusion thermodynamics of the materials, with occurrence of the shadowing effect. This phenomenon occurs when a high flow of powder onto the substrate surface absorbs most of the heat from the laser beam, preventing energy transfer for fusion of the substrate, resulting in depositions presenting a smaller fusion zone, less dilution, higher height values, and lower width values. Figure 14 shows a comparison of the height and width values for the depositions of the two materials. It can be seen that the AISI 316L stainless steel depositions were higher and narrower, compared to the AISI 431 depositions, confirming the influence of all these factors on the characteristics of the depositions.

3.6 Hardness Assays

Figure 15 shows the hardness values for the cross sections of the AISI 431 and AISI 316L depositions, considering the coating, the HAZ, and the substrate. For the AISI 431 stainless steel deposition, the highest hardness values were found in the coating zone, as expected. An average hardness value of 522 ± 4 HV$_{0.5}$ was obtained for the coating region, which was in agreement with the hardness of the material used to produce the deposition. The refinement of the structure due to the high cooling rate of the laser cladding process also contributed to greater hardness in the coating zone, as reported by Hemmati

et al. (Ref 9), Liu et al. (Ref 12), and Sun et al. (Ref 17). Higher hardness was observed in the HAZ, compared to the substrate, which was probably related to the diffusion of elements near the coating/substrate interface and/or refinement of the microstructure (Ref 11).

The coating zone of the AISI 316L deposition presented an average hardness of 356 ± 12 HV$_{0.5}$, in agreement with the hardness of AISI 316L stainless steel. As in the case of the AISI 431 deposition, the refinement of the microstructure due to the rapid cooling rate contributed to the high hardness values, as also observed by Sun et al. (Ref 15). The HAZ showed greater hardness than the substrate, which was also probably due to the diffusion of elements near the coating/substrate interface and/or refinement of the microstructure. In the substrate region, the average hardness values were 146 ± 5 HV$_{0.5}$ and 153 ± 3 HV$_{0.5}$ for the samples produced using the AISI 431 and AISI 316L stainless steels, respectively, in agreement with the hardness of ASTM A-36 carbon steel. As expected, the highest overall hardness values were obtained for the AISI 431 stainless steel depositions.

The hardness results indicated that there was no significant change in the mechanical properties of the materials, even for the highest dilutions. This demonstrated that under the conditions employed, the laser cladding process did not negatively affect the properties of the materials.

4. Conclusions

1. The characteristics of metal depositions produced using the laser cladding process, such as height, width, wetta-
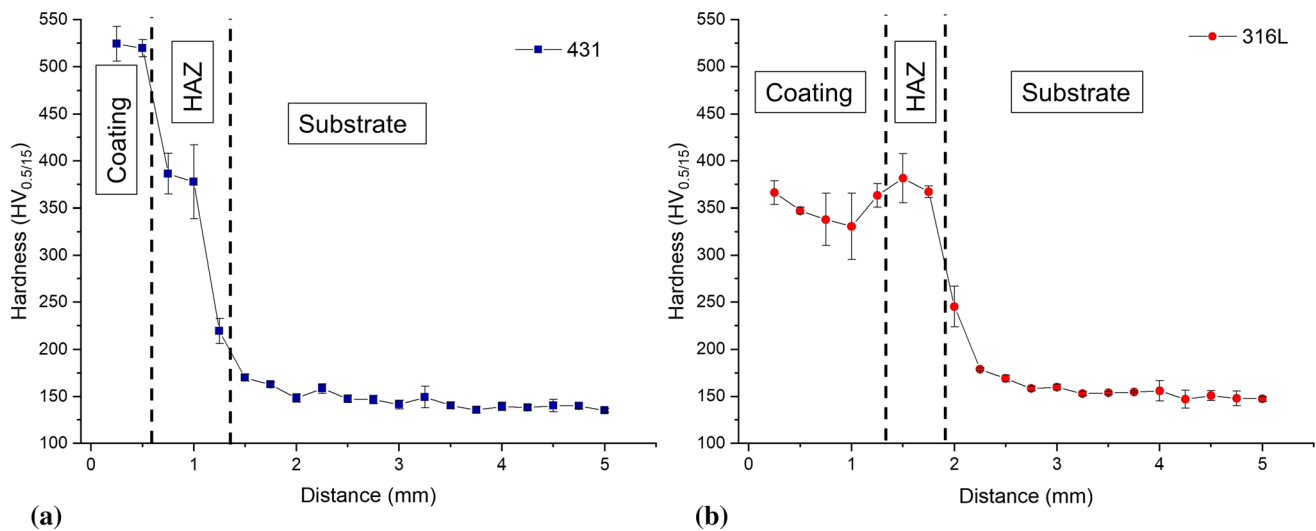
Fig. 15. Vickers hardness profiles of the AISI 431 (a) and AISI 316L (b) depositions

bility, and dilution, were influenced by process parameters including the laser beam power and scanning speed, metal particle morphology and size distribution, and addition metal powder flow rate.

2. The laser beam power and scanning speed had significant effects on the geometric and metallurgical characteristics of the depositions. The laser power was the main factor influencing the fusion zone, with higher power values leading to greater dilution and better wettability of the depositions.

3. For the AISI 431 stainless steel addition metal, the use of power values of 1400 and 1600 W, with scanning speeds of 9, 14, and 16 mm/s, enabled the formation of depositions with acceptable dilution values. The AISI 316L stainless steel addition metal required power values above 1900 W, at the same scanning speeds, in order to obtain satisfactory dilution values. Acceptable dilutions of between 10 and 20% were achieved for the depositions of both addition metals. For the AISI 316L addition metal, higher dilution values of between 15 and 41% were obtained using power values of 1900, 2100, 2400, and 2600 W.

4. Increase of the scanning speed resulted in greater dilution and wettability, together with a lower height/width ratio of the deposition. This was due to the change of the focal point of the powder flow relative to the focal point of the laser beam, which increased the laser beam energy on the substrate, consequently causing greater dilution. The decrease of the height/width ratio was associated with the lower powder flow per area, as the scanning speed was increased. It could also be concluded that the laser power had a greater influence on the width of the deposition, while the laser beam scanning speed had a greater effect on the deposition height.

5. The hardness tests revealed no significant changes in the hardness values of the materials used. For the AISI 431 stainless steel deposition, the coating region presented a mean hardness of 522 ± 4 HV$_{0.5}$, while a mean hardness of 356 ± 12 HV$_{0.5}$ was obtained for the of AISI 316L

deposition, in agreement with values reported in the literature.

References

1. F. Dehnavi, A. Eslami and F. Ashrafizadeh, A Case Study on Failure of Superheater Tubes in an Industrial Power Plant, *Eng. Fail. Anal.*, 2017, **80**, p 368–377. https://doi.org/10.1016/j.engfailanal.2017.07.007
2. Y. Liu, C. Liu, W. Liu, Y. Ma, S. Tang, C. Liang et al., Optimization of Parameters in Laser Powder Deposition AlSi10Mg Alloy Using Taguchi Method, *Opt. Laser Technol.*, 2019, **111**, p 470–480. https://doi.org/10.1016/j.optlastec.2018.10.030
3. V. Balasubramanian, A.K. Lakshminarayanan, R. Varahamoorthy and S. Babu, Application of Response Surface Methodolody to Prediction of Dilution in Plasma Transferred Arc Hardfacing of Stainless Steel on Carbon Steel, *J. Iron Steel Res. Int.*, 2009, **16**, p 44–53. https://doi.org/10.1016/S1006-706X(09)60009-1
4. F.S. da Luz, W.A. Pinheiro, S.N. Monteiro, V.S. Candido and A.C.R. da Silva, Mechanical Properties and Microstructural Characterization of a Novel 316L Austenitic Stainless Steel Coating on A516 Grade 70 Carbon Steel Weld, *J. Market. Res.*, 2020, **9**, p 636–640. https://doi.org/10.1016/j.jmrt.2019.11.004
5. S. Singh, K. Goyal and R. Goyal, Performance of Ni$_3$Al and TiO$_2$ Coatings on T$_{22}$ Boiler Tube Steel in Simulated Boiler Environment in Laboratory, *J. Mech. Eng.*, 2017, **46**, p 54–61. https://doi.org/10.3329/jme.v46i1.32524
6. I. Hemmati, V. Ocelik and J.T.M. De Hosson, Microstructural Characterization of AISI 431 Martensitic Stainless Steel Laser-Deposited Coatings, *J. Mater. Sci.*, 2011, **46**, p 3405–3414
7. L.H.R. Apolinario, D. Wallerstein, M.A. Montealegre, S.L. Urtiga Filho, E.A. Torres, T.F.C. Hermenegildo et al., Predominant Solidifi-

cation Modes of 316 Austenitic Stainless Steel Coatings Deposited by Laser Cladding on 304 Stainless Steel Substrates, *Metall. Mater. Trans. A*, 2019 https://doi.org/10.1007/s11661-019-05293-y

8. T.F.A. Santos and M.S. Andrade, Internal Friction on AISI 304 Stainless Steels with Low Tensile Deformations at Temperatures Between − 50 and 20 C, *Adv. Mater. Sci. Eng.*, 2010, **2010**, p 1–8. https://doi.org/10.1155/2010/326736

9. I. Hemmati, V. Ocelík and JTh.M. De Hosson, The Effect of Cladding Speed on Phase Constitution and Properties of AISI 431 Stainless Steel Laser Deposited Coatings, *Surf. Coat. Technol.*, 2011, **205**, p 5235–5239. https://doi.org/10.1016/j.surfcoat.2011.05.035

10. M. Moradi, H. Arabi, S. Jamshidi Nasab and K.Y. Benyounis, A Comparative Study of Laser Surface Hardening of AISI 410 and 420 Martensitic Stainless Steels by Using Diode Laser, *Opt. Laser Technol.*, 2019, **111**, p 347–357. https://doi.org/10.1016/j.optlastec.2018.10.013

11. M. Sharifitabar and A. Halvaee, Resistance Upset Butt Welding of Austenitic to Martensitic Stainless Steels, *Mater. Des.*, 2010, **31**, p 3044–3050. https://doi.org/10.1016/j.matdes.2010.01.026

12. Y. Liu, A. Li, X. Cheng, S.Q. Zhang and H.M. Wang, Effects of Heat Treatment on Microstructure and Tensile Properties of Laser Melting Deposited AISI 431 Martensitic Stainless Steel, *Mater. Sci. Eng., A*, 2016, **666**, p 27–33. https://doi.org/10.1016/j.msea.2016.04.014

13. M. Moradi, A. Ashoori and A. Hasani, Additive Manufacturing of Stellite 6 Superalloy by Direct Laser Metal Deposition—Part 1: Effects of Laser Power and Focal Plane Position, *Opt. Laser Technol.*, 2020, **131**, p 106328. https://doi.org/10.1016/j.optlastec.2020.106328

14. M. Moradi, A. Hasani, Z. Malekshahi Beiranvand and A. Ashoori, Additive Manufacturing of Stellite 6 Superalloy by direct Laser Metal Deposition—Part 2: Effects of Scanning Pattern and Laser Power Reduction in Different Layers, *Opt. Laser Technol.*, 2020, **131**, p 106455. https://doi.org/10.1016/j.optlastec.2020.106455

15. M. Nabhani, R.S. Razavi and M. Barekat, An Empirical-Statistical Model for Laser Cladding of Ti-6Al-4V Powder on Ti-6Al-4V Substrate, *Opt. Laser Technol.*, 2018, **100**, p 265–271. https://doi.org/10.1016/j.optlastec.2017.10.015

16. B.A. Khamidullin, I.V. Tsivilskiy, A.I. Gorunov and AKh. Gilmutdinov, Modeling of the Effect of Powder Parameters on Laser Cladding Using Coaxial Nozzle, *Surf. Coat. Technol.*, 2019, **364**, p 430–443. https://doi.org/10.1016/j.surfcoat.2018.12.002

17. G.F. Sun, X.T. Shen, Z.D. Wang, M.J. Zhan, S. Yao, R. Zhou et al., Laser Metal Deposition as Repair Technology for 316L Stainless Steel: Influence of Feeding Powder Compositions on Microstructure and Mechanical Properties, *Opt. Laser Technol.*, 2019, **109**, p 71–83. https://doi.org/10.1016/j.optlastec.2018.07.051

18. P. Aubry, C. Blanc, I. Demirci, M. Dal, T. Malot and H. Maskrot, Laser Cladding and Wear Testing of Nickel Base Hardfacing Materials: Influence of Process Parameters, *J. Laser Appl.*, 2017, **29**, p 022504. https://doi.org/10.2351/1.4983160

19. P. Alvarez, M. Montealegre, J. Pulido-Jiménez and J. Arrizubieta, Analysis of the Process Parameter Influence in Laser Cladding of 316L Stainless Steel, *J. Manuf. Mater. Process.*, 2018, **2**, p 55. https://doi.org/10.3390/jmmp2030055

20. C. Zhong, A. Gasser, J. Kittel, T. Schopphoven, N. Pirch, J. Fu et al., Study of Process Window Development for High Deposition-Rate Laser Material Deposition by Using Mixed Processing Parameters, *J. Laser Appl.*, 2015, **27**, p 032008. https://doi.org/10.2351/1.4919804

21. J. Näkki, J. Tuominen and P. Vuoristo, Effect of minor elements on solidification cracking and dilution of alloy 625 powders in laser cladding, *J. Laser Appl.*, 2017, **29**, p 012014. https://doi.org/10.2351/1.4973673

22. S. Katayama, Y. Kawahito and M. Mizutani, Elucidation of Laser Welding Phenomena and Factors Affecting Weld Penetration and Welding Defects, *Phys. Procedia*, 2010, **5**, p 9–17. https://doi.org/10.1016/j.phpro.2010.08.024

23. S.E. Aghili and M. Shamanian, Investigation of Powder Fed Laser Cladding of NiCr-Chromium Carbides Single-Tracks on Titanium Aluminide Substrate, *Opt. Laser Technol.*, 2019, **119**, p 105652. https://doi.org/10.1016/j.optlastec.2019.105652

24. A. Aggarwal, S. Patel and A. Kumar, Selective Laser Melting of 316L Stainless Steel: Physics of Melting Mode Transition and Its Influence on Microstructural and Mechanical Behavior, *JOM*, 2019, **71**, p 1105–1116. https://doi.org/10.1007/s11837-018-3271-8

25. J. Metelkova, Y. Kinds, K. Kempen, C. de Formanoir, A. Witvrouw and B. Van Hooreweder, On the Influence of Laser Defocusing in Selective Laser Melting of 316L, *Addit. Manuf.*, 2018, **23**, p 161–169. https://doi.org/10.1016/j.addma.2018.08.006

26. D.M. Goodarzi, J. Pekkarinen and A. Salminen, Effect of Process Parameters in Laser Cladding on Substrate Melted Areas and the Substrate Melted Shape, *J. Laser Appl.*, 2015, **27**, p S29201. https://doi.org/10.2351/1.4906376

27. M. Moradi and M. KaramiMoghadam, High Power Diode Laser Surface Hardening of AISI 4130; Statistical Modelling and Optimization, *Opt. Laser Technol.*, 2019, **111**, p 554–570. https://doi.org/10.1016/j.optlastec.2018.10.043

28. K. Shah, A.J. Pinkerton, A. Salman and L. Li, Effects of Melt Pool Variables and Process Parameters in Laser Direct Metal Deposition of Aerospace Alloys, *Mater. Manuf. Processes*, 2010, **25**, p 1372–1380. https://doi.org/10.1080/10426914.2010.480999

29. R.M. Miranda, G. Lopes, L. Quintino, J.P. Rodrigues and S. Williams, Rapid Prototyping with High Power Fiber Lasers, *Mater. Des.*, 2008, **29**, p 2072–2075. https://doi.org/10.1016/j.matdes.2008.03.030

30. H. Pajukoski, J. Näkki, S. Thieme, J. Tuominen, S. Nowotny and P. Vuoristo, High Performance Corrosion Resistant Coatings by Novel Coaxial Cold- and Hot-Wire Laser Cladding Methods, *J. Laser Appl.*, 2016, **28**, p 012011. https://doi.org/10.2351/1.4936988

31. L. Benedetti, B. Brulé, N. Decraemer, K.E. Evans and O. Ghita, Evaluation of Particle Coalescence and its Implications in Laser Sintering, *Powder Technol.*, 2019, **342**, p 917–928. https://doi.org/10.1016/j.powtec.2018.10.053

32. D. Riabov and S. Bengtsson. Factors Affecting Printability of 316L Powders Using the DMLS Process, September 16 (Beijing, China), *World Conference on Powder Metallurgy, China Powder Metallurgy Alliance*, 2018, p 1–12

33. B. Al-Mangour Ed., *Powder Metallurgy of Stainless Steel: State-of-the Art, Challenges, and Development. Stainless Steel: Microstructure*, Mechanical Properties and Methods of Application. Nova Science Publishers, New York, 2015, p 37–80

34. H. El Cheikh, B. Courant, S. Branchu, J.-Y. Hascoët and R. Guillén, Analysis and Prediction of Single Laser Tracks Geometrical Characteristics in Coaxial Laser Cladding Process, *Opt. Lasers Eng.*, 2012, **50**, p 413–422. https://doi.org/10.1016/j.optlaseng.2011.10.014

35. C. Zhong, T. Biermann, A. Gasser and R. Poprawe, Experimental Study of Effects of Main Process Parameters on Porosity, Track Geometry, Deposition Rate, and Powder Efficiency for High Deposition Rate Laser Metal Deposition, *J. Laser Appl.*, 2015, **27**, p 042003. https://doi.org/10.2351/1.4923335

36. D.J. Corbin, A.R. Nassar, E.W. Reutzel, A.M. Beese and N.A. Kistler, Effect of Directed Energy Deposition Processing Parameters on Laser Deposited Inconel ® 718: External Morphology, *J. Laser Appl.*, 2017, **29**, p 022001. https://doi.org/10.2351/1.4977476

37. M. Ansari, R. Shoja Razavi and M. Barekat, An empirical-Statistical Model for Coaxial Laser Cladding of NiCrAlY Powder on Inconel 738 Superalloy, *Opt. Laser Technol.*, 2016, **86**, p 136–144. https://doi.org/10.1016/j.optlastec.2016.06.014

38. J.A. Aguilera, C. Aragón and F. Peñalba, Plasma Shielding Effect in Laser Ablation of Metallic Samples and its Influence on LIBS Analysis, *Appl. Surf. Sci.*, 1998, **127–129**, p 309–314. https://doi.org/10.1016/S0169-4332(97)00648-X

39. J.M. Vadillo, J.M. Fernandez Romero, C. Rodríguez and J.J. Laserna, Effect of Plasma Shielding on Laser Ablation Rate of Pure Metals at Reduced Pressure, *Surf. Interface Anal.*, 1999, **27**, p 1009–1015

40. J. Xu, Y. Luo, L. Zhu, J. Han, C. Zhang and D. Chen, Effect of Shielding Gas on the Plasma Plume in Pulsed Laser Welding, *Measurement*, 2019, **134**, p 25–32. https://doi.org/10.1016/j.measurement.2018.10.047

41. L. Costa, I. Felde, T. Réti, Z. Kálazi, R. Colaço, R. Vilar et al., A Simplified Semi-Empirical Method to Select the Processing Parameters

for Laser Clad Coatings, *MSF*, 2003, **414–415**, p 385–394. https://doi.org/10.4028/www.scientific.net/MSF.414-415.385

42. J. Pekkarinen, A. Salminen, V. Kujanpää, J. Ilonen, L. Lensu and H. Kälviäinen, Powder Cloud Behavior in Laser Cladding Using Scanning Optics, *J. Laser Appl.*, 2016, **28**, p 032007. https://doi.org/10.2351/1.4947598

43. U. de Oliveira, V. Ocelík and JTh.M. De Hosson, Analysis of Coaxial Laser Cladding Processing Conditions, *Surf. Coat. Technol.*, 2005, **197**, p 127–136. https://doi.org/10.1016/j.surfcoat.2004.06.029

44. C. Bonnet, F. Valiorgue, J. Rech and H. Hamdi, Improvement of the Numerical Modeling in Orthogonal Dry Cutting of an AISI 316L Stainless Steel by The Introduction of a New Friction Model, *CIRP J. Manuf. Sci. Technol.*, 2008, **1**, p 114–118. https://doi.org/10.1016/j.cirpj.2008.09.006

45. Online Materials Information Resource - MatWeb 2021. http://www.matweb.com/index.aspx (accessed May 1, 2021)

46. D. Tanigawa, N. Abe, M. Tsukamoto, Y. Hayashi, H. Yamazaki, Y. Tatsumi et al., The Effect of Particle Size on the Heat Affected Zone During Laser Cladding of Ni–Cr–Si–B Alloy on C45 Carbon Steel, *Opt. Lasers Eng.*, 2018, **101**, p 23–27. https://doi.org/10.1016/j.optlaseng.2017.09.021

Publisher's Note Springer Nature remains neutral with regard to jurisdictional claims in published maps and institutional affiliations.